ATOMISTIC SIMULATIONS OF Ti ADDITIONS TO NiAl

GUILLERMO BOZZOLO*, RONALD D. NOEBE**, ANITA GARG**
JOHN FERRANTE** AND CARLOS AMADOR***
* Analex Corporation, 3001 Aerospace Parkway, Brook Park, OH, 44142-1003
**National Aeronautics and Space Administration, Lewis Research Center, Cleveland, OH 44135.
*** Facultad de Química, Universidad Nacional Autónoma de México, Ciudad Universitaria, 04510 Distrito Federal, México

ABSTRACT

The development of more efficient engines and power plants for future supersonic transports depend on the advancement of new high-temperature materials with temperature capabilities exceeding those of Ni-based superalloys. Having theoretical modelling techniques to aid in the design of these alloys would greatly facilitate this development. The present paper discusses a successful attempt to correlate theoretical predictions of alloy properties with experimental confirmation for ternary NiAl-Ti alloys. The B.F.S. (Bozzolo- Ferrante-Smith) method for alloys is used to predict the solubility limit and site preference energies for Ti additions of 1 to 25 at. % to NiAl. The results show the solubility limit to be around 5 % Ti, above which the formation of Heusler precipitates is favored. These results were confirmed by transmission electron microscopy performed on a series of NiAl-Ti alloys.

Introduction

Ordered intermetallic compounds and in particular the B2 structured NiAl have long been considered as prime candidates to replace superalloys in the combustion and turbine sections of jet engines but inadequate creep and fracture resistance are a concern. One of the most basic strategies for improving creep resistance is to combine single crystal processing with alloying of reactive elements such as Ti, Hf, Zr and Ta [1]. This approach has been so effective that single crystal NiAl alloy turbine vanes have been successfully engine tested [2]. These reactive elements generally have a low solubility in NiAl and precipitate as various intermetallic phases, e.g., Heusler (Ni_2AlX) and Laves (NiAlX) phases. NiAl-Ni_2AlTi alloys have greater creep strength than either constituent phase [3], and are comparable in strength to Ni-based superalloys. More impressive is the effect that these reactive elements have on the strength of NiAl when at levels below their solubility limit. For example, Ti additions on the order of 2.5-3 at. % result in a 200-5000 fold reduction in creep rate over binary NiAl single crystals [4]. The mechanism behind this large solid solution strengthening effect in NiAl is presently unclear and complete understanding of this phenomenon, and in general the optimization of NiAl-Heusler alloys, is hampered by the lack of detailed structural information concerning the NiAl-Ti system. Consequently, owing to the engineering significance of Ni-rich NiAl-Ti alloys [1,2] and in an effort to develop confidence in our modelling abilities, $Ni_{50}Al_{50-x}Ti_x$ alloys have been modeled by the BFS method for alloys and the results compared to a concurrent transmission electron microscopy study.

The BFS Method with First-Principles Input

The BFS method is based on dividing the energy of formation of an alloy in a superposition of

Mat. Res. Soc. Symp. Proc. Vol. 460 © 1997 Materials Research Society

LMTO parameters for pure bcc elements					BFS parameters for B2 A-B alloys		
Element	a_0 (Å)	E_C (ev/atom)	B_0 (GPa)	E_v (eV/atom)	A-B	$\Delta_{AB}(Å^{-1})$	$\Delta_{BA}(Å^{-1})$
Al(bcc)	3.192	3.945	77.3	1.8	Ni Al	-0.05813	0.0822
Ni(bcc)	2.752	5.869	249.2	3.0	Ti Al	0.2283	-0.06360
Ti(bcc)	3.213	6.270	121.0	2.0	Ni Ti	-0.06587	0.4610

Table 1: LMTO results for the lattice parameter, cohesive energy, bulk modulus and vacancy formation energy for the bcc phases of Ni, Al and Ti. The last three columns display the ensuing BFS parameters determined from LMTO results.

individual contributions ϵ_i of non-equivalent atoms in the alloy [5]:

$$\epsilon_i = \epsilon_i^S + g_i(\epsilon_i^C - \epsilon_i^{C_0}). \tag{1}$$

ϵ_i has two components: a *strain* energy ϵ^S, computed with equivalent crystal theory (ECT) [6], that accounts for the actual geometrical distribution of the atoms surrounding atom i, computed as if all its neighbors were of the same atomic species, and a *chemical* energy $\epsilon^C - \epsilon^{C_0}$, which takes into account the fact that some of the neighbors of atom i may be of a different chemical species. For ϵ_i^C we interpret the chemical composition as a defect of an otherwise pure crystal. We represent this defect by 'perturbing' the electronic density in the overlap region between dissimilar atoms and locating them at equilibrium lattice sites of atom i. The ideas of ECT [6] are used to develop a procedure for the evaluation of the energy associated with this 'defect'. To free the chemical energy of structural defect energy which should only be included in the strain energy, we reference ϵ_i^C to a similar contribution where no such perturbation is included ($\epsilon_i^{C_0}$). The coupling function g_i, which ensures the correct asymptotic behavior of the chemical energy, is defined as $g_i = e^{-a_i^S}$, where a_i^S is a solution of $\epsilon_i^S = -E_C^i\left[1-(1+a_i^S)exp(-a_i^S)\right]$ (see ref. [5]), and where E_C^i is the cohesive energy for atom i. In the context of BFS, the terms 'strain' and 'chemical' represent quite different effects from the usually assigned meanings. For a clear understanding of this method, we direct the reader to Ref. 5 where a detailed description of the calculation of the strain and chemical energy contributions is provided. Except for two parameters determined by fitting to experimental or theoretical alloy properties, the method relies on pure element properties. The BFS parameters used in this work, as well as the ECT parameters are defined in refs. 5 and 6, respectively, and have been used in previous BFS applications with a great degree of success.

B.F.S. results for NiAl-Ti

Exploiting the computational simplicity of BFS, we defined a large number of Ni-Al-Ti lattices, covering a wide range of concentrations with different atomic distributions and different degrees and types of ordering for each composition. The approach used is to define a certain 'configuration', then use the BFS method to compute the energy of formation -as well as the lattice parameter and bulk modulus for that specific configuration of atoms- and then compare results for these configurations [7]. In doing so, we 1) relate general trends of the energy of formation and lattice parameter to changes in concentration and atomic distribution and 2) identify metastable structures, that is, configurations with energy close to that of the ground state, which might have a large probability of appearing in the actual alloy depending on conditions present during processing. Therefore, this 'catalog' of alternative configurations serves the purpose of identifying ordering trends, formation of precipitates, etc., as well as providing physical insight to the reason why a particular microstructure forms. If the set of configurations sampled (see Ref. 8 for details) is sufficiently large and the structures are chosen respecting the symmetries underlying the studied phase, one would expect to

find the equilibrium state or states sufficiently close to it for each composition. This approach is not meant to replace large scale Monte Carlo simulations which would provide the full description of the composition and temperature dependence of the ground state. On the contrary, it could be taken as a supplementary set of calculations which could enhance the somewhat limited information provided by Monte Carlo simulations. Results using Monte Carlo with BFS will be published elsewhere [8]. This sampling algorithm follows in spirit the comprehensive searches of ground states method [9].

Site preference: In general, those configurations where Ti atoms occupy sites in the Al sublattice are consistently lower in energy. Fig. 1 indicates - in an energy spectrum fashion - the energies of formation of configurations characterized by a certain substitutional defect: A(B) indicates an A atom occupying a site in the B sublattice whereas A(B)C indicates an A atom in a B site which in turn occupies a site in the C sublattice. Fig. 1 shows the corresponding results for three different Ti concentrations: 1.39, 2.78 and 6.94 at. % Ti, which correspond to 1, 2 and 5 Ti atoms respectively in a 72 atoms cell. For the first case, two configurations are possible: the Ti atom occupying an Al site or the Ti atom occupying a Ni site with the displaced Ni atom located in an Al site, which in turn could be located at nearest neighbor distance to the Ti atom (*NN*) or farther away (*far*). The Ti(Al) defect is clearly favorable. A similar situation is seen at higher concentrations (x_{Ti}=2.78) where, necessarily, more options are available for the relative location of the antistructure and substitutional atoms. The lowest energy corresponds to the Ti atoms located throughout the Al sites followed by an arrangement of atoms resulting in Heusler ordering, which in turn is followed by a random but closely aggregated distribution of Ti atoms in Al sites. Finally, at 6.94 at. % Ti, Heusler formation is favored over a solid solution NiAl-Ti alloy. Based on these results, the preference of Ti for Al sites is clear.

Solubility limit: However, once the whole set of configurations is analyzed in the same fashion - covering the whole range of Ti concentrations from 1 to 25 at. % and including all possible ordering patterns - a clear picture emerges regarding the behavior of Ti in NiAl. Fig. 2 indicates the results for the whole set of configurations considered in this work. While Fig. 1 concentrates on just three different concentrations and focuses on a few select configurations for each concentration, Fig. 2 expands on these results by showing the complete set of over 200 alloy configurations studied. One clear feature in Fig. 2 becomes immediately apparent: beyond 5 at. % Ti, there is a clear separation between a selected type of configurations (denoted with circles) and the rest (denoted with solid squares). Those configurations denoted by circles share a particular type of ordering, where Ti atoms locate themselves exclusively in Al sites -as expected - in such way that they form regions of alternating rows of Al and Ti atoms within Al planes. This ordering pattern corresponds to the $L2_1$ ordered structure or Heusler phase when the concentration of Ti is 25 %. At that concentration, the gap between this configuration (solid circle in Fig. 2) and any other one is a maximum, clearly indicating the stability of this phase, in agreement with experiment. Moreover, the BFS prediction for the lattice parameter (5.828 Å) is in excellent agreement with the experimental value (5.840 Å). At any given concentration, the rest of the configurations studied are much higher in energy in a direct proportionality to their degree of disorder while the lowest energy states are found to always contain some level of Heusler-type ordering. Another remarkable feature is clearly noticed when the configurations with Heusler-like ordering (open circles in Fig. 2) are compared to the next lower energy states: below 5 % Ti, those congifurations where Ti is in solid solution with the matrix are energetically favored, however so slightly (as demonstrated in Fig. 1) over those where short range order dominates. This situation is reversed above 5 % Ti, with an ever more distinguishable preference for Heusler ordering with increasing Ti concentration. In other words, Heusler ordering is preferred beyond a certain critical value near 5 at. % Ti. In processing the actual alloy, according to these results, Ti atoms in solid solution at high temperatures would therefore tend to stay in

such disordered state whereas above the critical value the formation of Heusler-like ordering in the form of Ni_2AlTi precipitates is favored. This crude way of determining the solubility limit of Ti in NiAl, not only establishes this critical value but it also provides some insight on the behavior of the system for a wide range of concentrations surrounding the solubility limit, in agreement with Monte Carlo simulations [8].

Transmission Electron Microscopy

Three NiAl single crystal alloys (Ni-47Al-3Ti, Ni-45Al-5Ti and Ni-43Al-7Ti) were grown by a Bridgman technique at the University of Florida. The ingots were homogenized for 32 hrs. at 1644 K, aged for 6 hrs. at 1255 K and slowly furnace cooled from the aging temperature. Samples for transmission electron microscopy (TEM) were prepared from 3mm diameter cylinders electro-discharge machined from the heat treated ingots. Slices sectioned from the cylinders were mechanically ground and electrochemically thinned in a twin-jet Tenupol-3 polisher. Microstructural (brighfield/darkfield) and diffraction analysis were conducted in a Phillips 400 T TEM equipped with a double tilt goniometer.

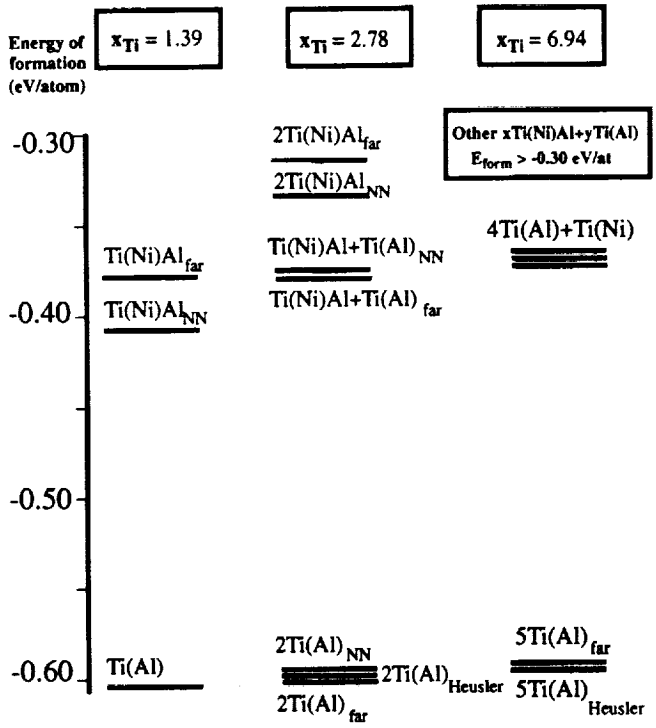

Fig. 1: Energies of formation (in eV/atom) for 72 atoms cells containing 36 Ni atoms, 36-x Al atoms and x Ti atoms (x = 1, 2, 5). The different energy states correspond to different substitutional defect schemes (see text).

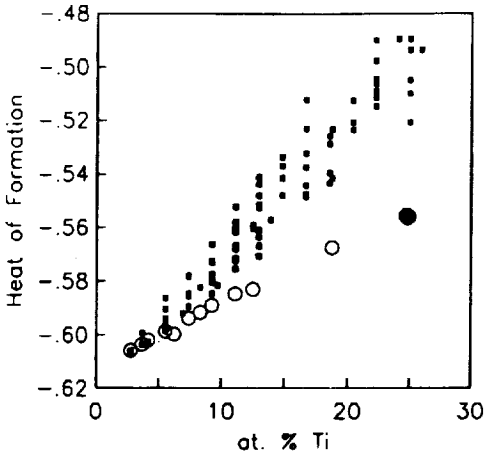

Fig. 2: Energy of formation (in eV/atom) for over 200 different NiAl-Ti alloys (see text).

Fig. 3 a) Bright-field TEM image of Ni-47Al-3Ti and b) corresponding (110) SADP. c) Dark-field TEM image of Ni-43Al-7Ti showing precipitation of Heusler particles and d) corresponding SADP. 001, 110 and 111 NiAl matrix spots are indicated on the diffraction pattern, which correspond to 002, 220 and 222 Heusler spots, respectively.

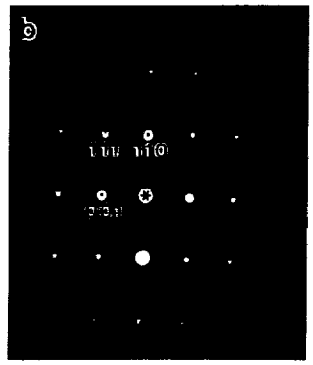

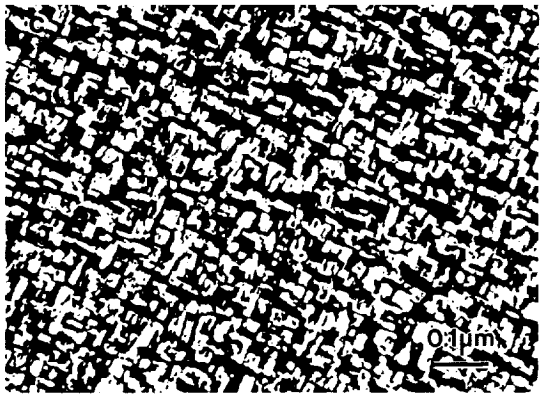

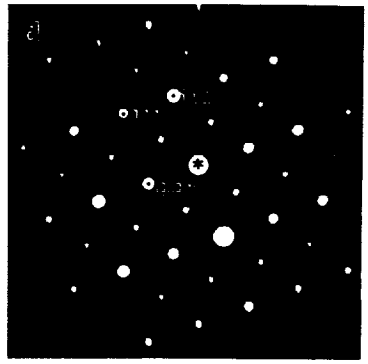

Microstructural characterization: Fig. 3.(a) shows a brightfield image of the Ni-47Al-3Ti. Except for an occasional dislocation, the microstructure is very clean and featureless and shows no sign of any second phase precipitation. This is confirmed in the corresponding (110) zone-axis selected area diffraction pattern (SADP), presented in Fig. 3.(b), which shows only the NiAl matrix spots and no extra spots due to precipitation. In contrast, Fig. 3.(c) shows a dark-field TEM image of the Ni-43Al-7Ti alloy after identical heat treatment. Precipitation of a high density of well defined precipitate plates ranging in size between 10-50 nm can be clearly seen. The corresponding (110) diffraction pattern (Fig. 3.(d)) shows distinct extra spots which were indexed to a fcc crystal structure with lattice parameter almost two times that of NiAl, i.e. $a_0 = 0.586$ nm, corresponding to the Heusler phase Ni_2AlTi. Fig. 3.d also indicates that the Ni_2AlTi phase nucleates with a cube-on-cube orientation relationship with the NiAl matrix phase, i.e $[110]_{NiAl}//[110]_{Ni_2AlTi}$,$(001)_{NiAl}//(001)_{Ni_2AlTi}$. Due to the small lattice misfit between the precipitate and NiAl phase, $\sim$1.5 %, the Heusler plates are still coherent with the matrix and in bright-field TEM views exhibit extensive coherency strains. Consistent with the analytical modeling results, which indicate that the solubility limit for Ti in NiAl at absolute zero temperature is near 5 %, the slow cooled Ni-45Al-5Ti alloy exhibited a microstructure similar to that of the 7Ti-alloy except that the average precipitate size was on the order of 1-5 nm. These results are fully consistent with the analytical results summarized in Figs. 1 and 2.

Conclusions

The B.F.S. method for alloys was used to successfully predict the experimentally verified solubility limit of Ti in NiAl and the formation of Heusler precipitates beyond the solubility limit. Moreover, the method succesfully predicts the stability of the Heusler phase at 25 % Ti, including an excellent approximation to the experimental value of the lattice parameter. This represents a significant success for the use of semiempirical atomistic methods for alloy design. The success of this and other studies hold the promise that the B.F.S. method will greatly facilitate the development of new alloys for aircraft and other applications.

References

[1] W. S. Walston, R. D. Field, J. R. Dobbs, D. F. Lahrman and R. Darolia, in Structural Intermetallics, R. Darolia et al. eds., The Minerals, Metals and Materials Society, 1993, pp. 523-532.

[2] R. Darolia, W. S. Walston and M. V. Nathal, in Superalloys 1996, R. D. Kissinger et al. eds., The Minerals, Metals and Materials Society, 1996, pp. 561-570.

[3] P. R. Strutt, R. S. Polvani and J. C. Ingram, Met. Trans. A, **7A** (1976) 23.

[4] W. D. Nix and R. H. Dauskardt, 'High Temperature Deformation and Fracture Resistance of Single Crystals of NiAl and NiAl-based Intermetallic Alloys', Annual Progress Report for AFOSR Grant No. AF-F49620-95-1-0163, Sept. 1996.

[5] G. Bozzolo and J. Ferrante, J. Computer-Aided Mater. Design, **1** (1993) 305, and references therein.

[6] J. R. Smith, T. Perry, A. Banerjea, J. Ferrante and G. Bozzolo, Phys. Rev. B **44** (1991) 6444.

[7] G. Bozzolo, C. Amador, J. Ferrante and R. D. Noebe, Scr. Met. Mater., **33** (1995) 1907.

[8] G. Bozzolo, R. Noebe and J. Ferrante, to be published.

[9] C. Wolverton, G. Ceder, D. de Fontaine and H. Dreysse, Phys. Rev. **B45** (1992) 13105.